

# Real-time Transmission of Geometrically-shaped Signals using a Software-defined GPU-based Optical Receiver

Sjoerd van der Heide, *Student Member, IEEE*, Ruben S. Luis, *Senior Member, IEEE*, Sebastiaan Goossens, *Student Member, IEEE*, Benjamin J. Puttnam, *Member, IEEE*, Georg Rademacher, *Senior Member, IEEE*, Ton Koonen, *Fellow, IEEE*, Satoshi Shinada, *Member, IEEE*, Yohinari Awaji, *Member, IEEE*, Alex Alvarado, *Senior Member, IEEE*, Hideaki Furukawa, *Member, IEEE*, Chigo Okonkwo, *Senior Member, IEEE*

(Top Scored)

**Abstract**—A software-defined optical receiver is implemented on an off-the-shelf commercial graphics processing unit (GPU). The receiver provides real-time signal processing functionality to process 1 GBaud minimum phase (MP) 4-, 8-, 16-, 32-, 64-, 128-ary quadrature amplitude modulation (QAM) as well as geometrically shaped (GS) 8- and 128-QAM signals using Kramers-Kronig (KK) coherent detection. Experimental validation of this receiver over a 91 km field-deployed optical fiber link between two Tokyo locations is shown with detailed optical signal-to-noise ratio (OSNR) investigations. A net data rate of 5 Gbps using 64-QAM is demonstrated.

**Index Terms**—Real-time, GPU, field-deployed link, Kramers-Kronig, geometric shaping.

## I. INTRODUCTION

In recent years, graphics processing units (GPUs) have been proposed as an alternative to field-programmable gate arrays (FPGAs) [1]–[3] and application-specific integrated circuits (ASICs) for optical communications [4]–[12]. More than a decade of steady exponential improvement of computation capacity (45% yearly increase [13]) and energy efficiency (25% yearly increase [14]) of GPUs have accelerated its potential applications in the field of optical communications. Recent demonstrations include real-time forward error correction (FEC) decoding [4], [5], physical-layer functionality [6]–[8], differential quaternary phase-shift-keying (DQPSK) detection [9], and flexible multi-modulation format detection using directly detected pulse-amplitude modulated signals,

and coherently detected quadrature amplitude modulation (QAM) signals [10]–[12] using Kramers-Kronig (KK) detection [15]. The real-time receiver has been demonstrated over a 10,000 km straight-line link [12] and a field-deployed fiber [11].

In this work, we extend the flexible, software-defined real-time multi-modulation format receiver with geometric shaping (GS). A commercial off-the-shelf GPU is used for real-time digital signal processing of minimum phase (MP) 4-, 8-, 16-, 32-, 64-, and 128-QAM as well as geometrically-shaped 8-QAM and 128-QAM signals using KK coherent detection [15]. The receiver is experimentally validated using a field-deployed transmission link between two Tokyo locations. Detailed investigations into optical signal-to-noise ratio (OSNR) performance are shown and carrier-to-signal power ratio (CSPR) is optimized for all transmission scenarios. Net throughput is calculated for the evaluated formats and multiple hard decision forward error correction (HD-FEC) algorithms, with 64-QAM paired with a 20% overhead HD-FEC achieving a net throughput of 5 Gbps at 24.1 dB OSNR.

This paper is an extension to the work presented at the European Conference on Optical Communication (ECOC 2020) [10]. Extended results using the field trial link including reconfigurable optical add-drop multiplexers (ROADMs) and both N-ary pulse-amplitude modulation (PAM) intensity-modulation direct-detection (IM/DD) and KK coherent N-QAM formats are presented in [11]. Compared to our earlier work, we employ the same field-deployed link but without ROADMs in order to demonstrate GS-N-QAM transmission and further investigate the influence of CSPR. In addition, a higher bandwidth receiver is used, leading to increased performance and demonstration of higher cardinality modulation formats including 128-QAM. The paper is structured as follows: Section II describes the implemented real-time GPU-based digital signal processing (DSP) chain. Section III describes the experimental setup in detail and Section IV describes the results. A discussion of the work is presented in Section V and Section VI concludes this paper.

Sjoerd van der Heide, Ton Koonen, and Chigo Okonkwo are with the High Capacity Optical Transmission Laboratory, Electro-Optical Communications Group, Eindhoven University of Technology, PO Box 513, 5600 MB, Eindhoven, the Netherlands. (e-mail: s.p.v.d.heide@tue.nl, c.m.okonkwo@tue.nl, a.m.j.koonen@tue.nl). Ruben S. Luis, Benjamin J. Puttnam, Georg Rademacher, Satoshi Shinada, Yohinari Awaji, and Hideaki Furukawa are with the National Institute of Information and Communications Technology, Photonic Network System Laboratory, 4-2-1, Nukui-Kitamachi, Koganei, Tokyo, 184-8795, Japan (e-mail: rluis@nict.go.jp). Sebastiaan Goossens and Alex Alvarado are with the Information and Communication Theory Lab, Signal Processing Systems Group, Department of Electrical Engineering, Eindhoven University of Technology, Eindhoven, the Netherlands (e-mail: s.a.r.goossens@tue.nl, a.alvarado@tue.nl).

Manuscript received xxxx; revised xxxx; accepted xxxx. Date of publication xxxx. This work was partly supported by the Dutch NWO Gravitation Program on Research Center for Integrated Nanophotonics under Grant GA 024.002.033.

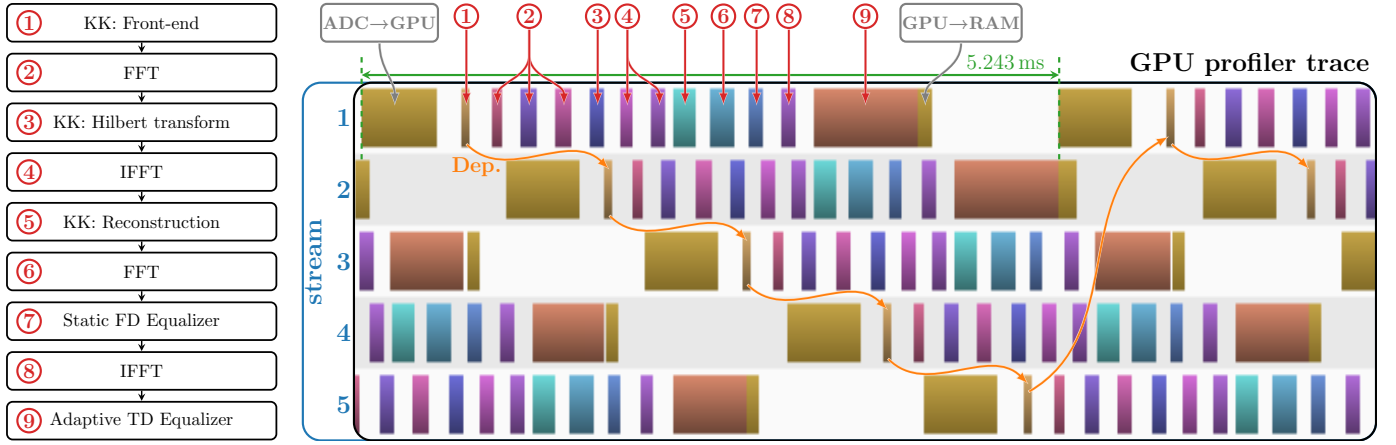


Fig. 1: Real-time Kramers-Kronig digital signal processing chain including GPU profiler trace, additional details in [11].

## II. DIGITAL SIGNAL PROCESSING CHAIN

Fig. 1 shows the real-time DSP chain for KK coherent N-QAM signals. Here, an overview of its GPU-based implementation is given. A more detailed description can be found in [11]. First, buffers containing  $2^{22}$  digitized samples are transferred from analog-to-digital converter (ADC) to GPU in real time using direct memory access (DMA). The signal processing starts with a GPU kernel converting samples received as 12-bit fixed point to 32-bit floating point numbers, adding the appropriate DC offset, and performing the square root and logarithm KK front-end operations. This first kernel is annotated by the number 1 in Fig. 1. In step 3, enabled by a pair of 100% overlap-save 1024-point fast Fourier transforms (FFTs), the phase of the optical signal is recovered by a frequency-domain Hilbert transform. This phase is combined with the amplitude calculated in step 1 to reconstruct the optical signal [15] which is subsequently downconverted for further processing. Another pair of FFTs supports frequency-domain static equalization and resampling from 4 to 2 samples-per-symbol. Finally, a 4-tap adaptive time-domain widely-linear [16] decision-directed least mean square (DD-LMS) equalizer is employed to recover the signal. The decisions made by the equalizer are demapped into bits and sent to random-access memory (RAM).

Full utilization of GPU resources is achieved through massive parallelization within kernels as well as operating multiple processing streams in parallel. Most of the kernels operating within each stream are highly parallel themselves, e.g. the FFTs, Hilbert transform, and the frequency-domain equalizer. However, algorithms such as the adaptive time-domain equalizer are hard to parallelize due to its sequential nature and time-dependencies of the tap updates. The use of multiple processing streams allows these hard-to-parallelize algorithms to run next to easy-to-parallelize algorithms. Therefore, even though the adaptive equalization takes up significant amount of *time* as shown in the GPU profiler trace in Fig. 1, significant amount of *resources* is not required. This concept and many other implementation strategies are discussed in detail in [11].

Note that several parameters of the real-time receiver are

static and optimized offline. Since the ADC is AC-coupled, the DC-term of the signal is lost. This DC-term is crucial for correct signal reconstruction and is added in step 1 as described above. The question remains how to determine the optimal value since it is dependent on the signal power, noise power, and CSNR. Throughout this work, all measurements are performed multiple times using different DC offset values to ensure the optimal performance is observed. Alternatively, one could implement an algorithm to calculate and update the optimal DC-term in real-time [17].

Similarly, the static frequency-domain equalizer is optimized offline using a training sequence. Therefore, the entire signal processing chain up to the adaptive equalizer is agnostic to the modulation employed. Only the adaptive equalizer needs to know the constellation since, after initial setup and convergence using a training sequence, it is updated in a blind decision-directed fashion. Also, these symbol decisions are demapped into bits and are considered as the output of the DSP chain. The constellation points and bit mapping are uploaded to the GPU for the equalizer to make decisions based on a minimum Euclidean distance criterion. Support for various geometrically-shaped constellations is achieved by simply uploading the location of the constellation points and corresponding bit mapping.

## III. EXPERIMENTAL SETUP

Fig. 2 shows the experimental setup using the field-deployed link between Koganei and Otemachi, Tokyo. First, a 12 GS/s arbitrary-waveform generator (AWG) generates MP 1 GBaud QAM signals with 1% rolloff root-raised-cosine (RRC) pulse shaping with a digitally inserted carrier tone at 0.516 GHz. Both conventional and geometrically shaped QAM formats are employed, the latter optimized for the additive white Gaussian noise (AWGN) channel and generated through an iterative optimization process similar to [18]. Further details can be found in Section V.

An in-phase and quadrature modulator (IQM) modulates the signal onto a 100 kHz linewidth 1550.51 nm external cavity laser (ECL). The amplified signal is launched into 45.5 km of field-deployed standard single-mode fiber (SSMF) at a

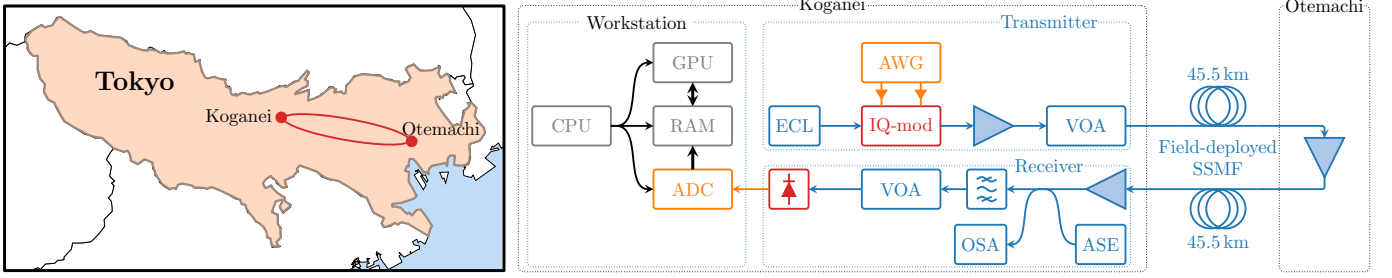


Fig. 2: Experimental setup with a field-deployed link between Koganei and Otemachi, Tokyo, Japan.

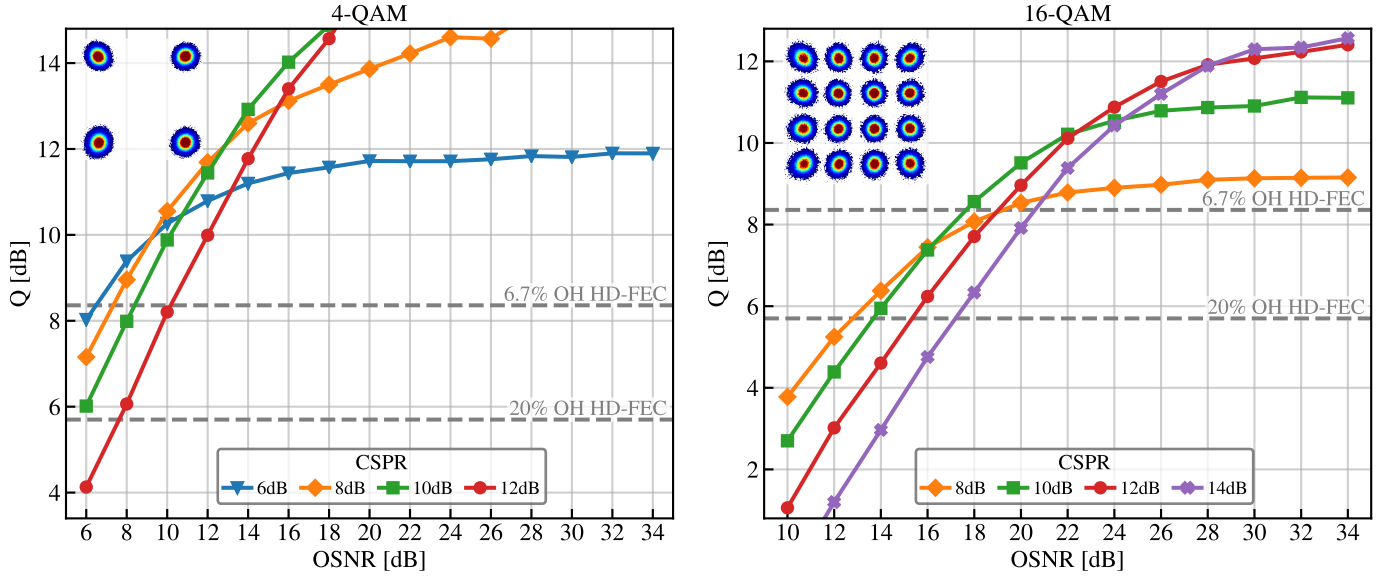


Fig. 3: Q-factor versus OSNR for 4-QAM and 16-QAM for various CSRs.

fixed launch power. At the other location in Otemachi, Tokyo, an erbium-doped fiber amplifier (EDFA) amplifies the signal again to the same launch power and it is transmitted back to Koganei via 45.5 km of SSF. 56% of this fiber is installed in underground ducts and the remainder on aerial paths and in the surface along railway tracks.

At the receiver, the signal is amplified, combined with amplified spontaneous emission (ASE) from a noise-loading stage to vary the OSNR, and filtered using a 5 GHz bandpass filter (BPF). A variable optical attenuator (VOA) controls the optical power into the 6.5 GHz photodiode such that the electrical output swing fills the 1 GHz 4 GS/s ADC detection range. Receiver DSP is performed in real-time on the GPU as described in Section II.

Several optimizations have been employed to increase OSNR performance. Firstly, no significant dependence of launch power on OSNR performance was observed. Therefore, the launch power was fixed. Next, the gap between the digitally-inserted carrier required for KK detection was optimized. With the 1% roll-off RRC 1 GBaud signal ending at 0.505 GHz and the carrier tone at 0.516 GHz, a gap of only 11 MHz was left. One would expect a larger gap to be more beneficial since it reduces signal-signal beat interference (SSBI) which when not entirely removed by the KK algorithm leaves reconstruction errors. However, the ADC has a

bandwidth of 1 GHz, thus impairing the signal after detection but crucially before the KK algorithm, leading to imperfect reconstruction. It is expected that this penalty from increased imperfect reconstruction obstructs the use of a larger gap. Finally, the power of the carrier tone relative to the signal, the CSRP, is varied and reported on in the next section.

#### IV. RESULTS

Fig. 3 shows the Q-factor versus OSNR for 4-QAM and 16-QAM for multiple CSRs. It is clear that lower CSR values perform better in the low OSNR regime and higher CSRs at higher OSNR. Note that total signal power as defined in the OSNR includes both the carrier tone and the N-QAM signal. Therefore, if CSR is increased, signal power decreases, signal-to-noise ratio (SNR) decreases, and Q-factor decreases. This is especially relevant at low OSNRs. Conversely, if CSR is increased, carrier power increases, SSBI decreases, fewer reconstruction errors occur, and Q-factor increases. This is relevant at higher OSNRs. The CSR trade-off between noise and reconstruction errors is observed for all tested modulations.

4-QAM with 6 dB CSR reaches the 6.7% overhead HD-FEC Q-factor threshold of 8.36 dB [19] at 6.5 dB OSNR. For this specific CSR, the Q-factor never exceeds 12 dB whilst higher CSRs have a lower error floor or Q-factor

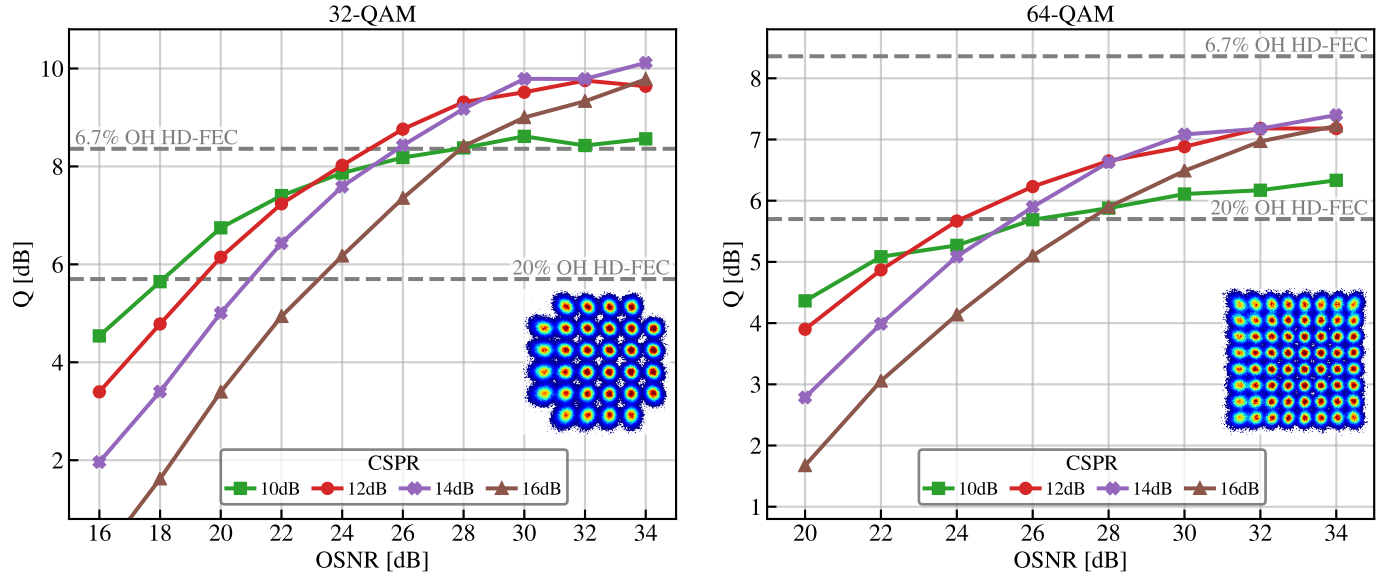


Fig. 4: Q-factor versus OSNR for 32-QAM and 64-QAM for various CSPRs.

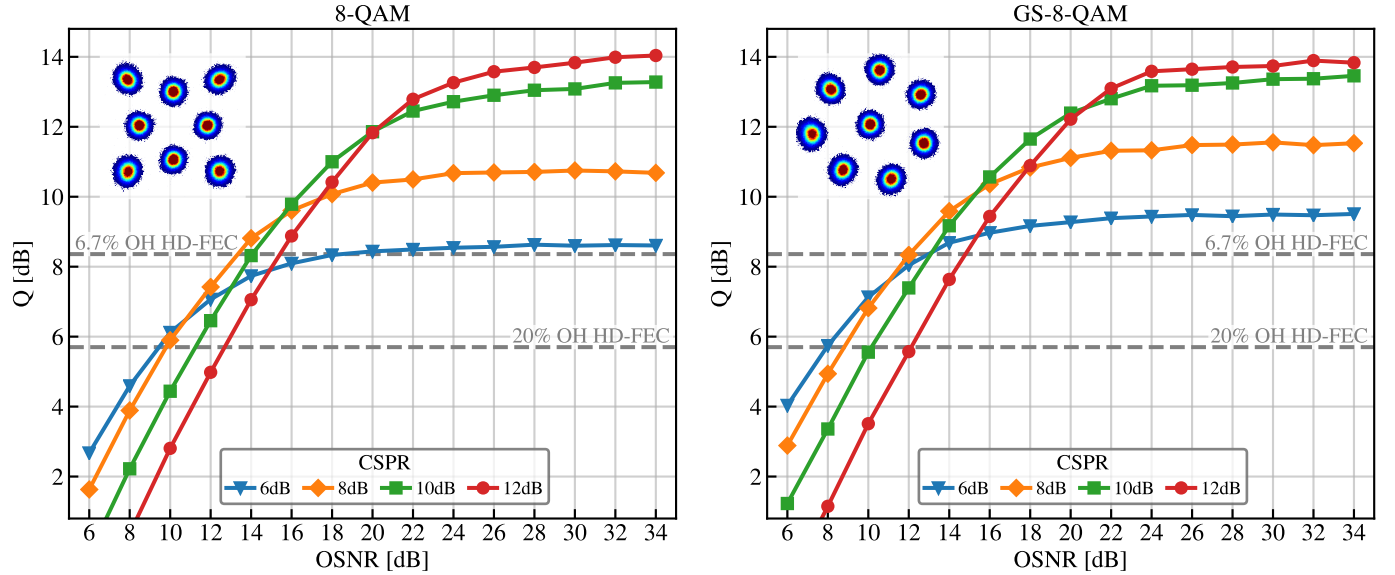


Fig. 5: Q-factor versus OSNR for 8-QAM and GS-8-QAM for various CSPRs.

ceiling. The optimal CSPR depends on the operating regime of the transmission link, the modulation format, and the FEC algorithm employed. Q-values above 15 dB are not displayed in Fig. 3 because too few errors were recorded for statistical significance. 16-QAM reaches the 20% overhead HD-FEC Q-factor threshold of 5.70 dB [19] at 12.8 dB OSNR using a CSPR of 8 dB. The 6.7% overhead HD-FEC is reached at 17.8 dB using 10 dB CSPR.

OSNR performance for 32-QAM and 64-QAM are shown in Fig. 4. 32-QAM is able to reach both the 20% and 6.7% overhead FEC limit at 18.1 dB and 24.9 dB, respectively. However, 64-QAM is not able to reach the 6.7% overhead FEC threshold, but reaches the other threshold at 24.1 dB.

Fig. 5 depicts the OSNR performance for both conventional and geometrically-shaped 8-QAM. The GS format out-

performs its conventional counterpart and reaches the 6.7% overhead threshold at 12.0 dB versus 13.3 dB for the conventional format. Similarly, at the 20% threshold, GS-8-QAM outperforms 8-QAM by 1.6 dB and reaches the threshold at 7.9 dB compared to 9.5 dB for 8-QAM.

Fig. 6 shows the Q-factor as a function of OSNR for all evaluated modulation formats aggregated in one figure. For each OSNR, the highest measured Q-factor for that modulation format is plotted, effectively tracing a line along the maximum Q-factor of each modulation format in Figs. 3 to 5 and 128- and GS-128-QAM. As a result, CSPR is optimized for each OSNR. Using this optimization approach, 4-, GS-8-, 8-, 16-, and 32-QAM reach the 6.7% HD-FEC threshold. 64-QAM only reaches the 20% HD-FEC threshold, but 128- and GS-128-QAM unfortunately stay below the thresholds.

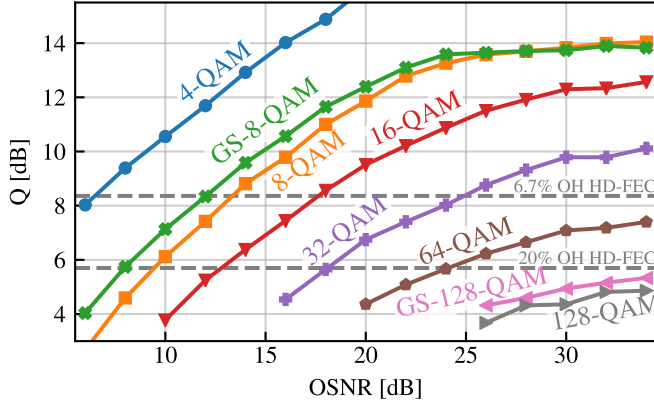


Fig. 6: Q-factor versus OSNR for all evaluated modulation formats at optimized CSNR.

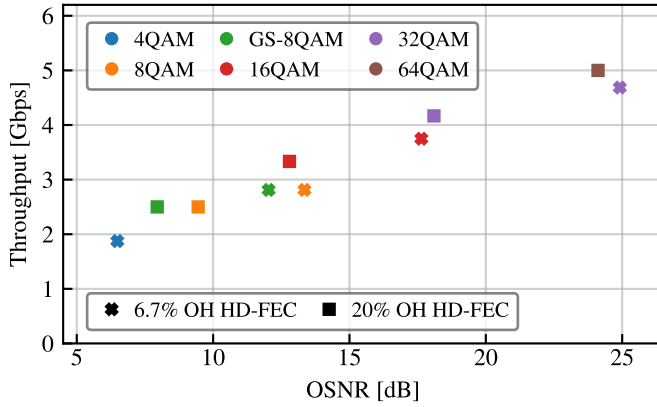


Fig. 7: Net throughput as a function of OSNR for the evaluated modulation formats and HD-FEC thresholds.

Fig. 7 estimates the net throughput of the transmission system at various OSNRs. For each of the HD-FEC threshold crossings mentioned above, the net data rate after FEC decoding at the OSNR of the crossing is plotted. This figure reveals interesting choices for the system designer. If the system operates at 25 dB, 64-QAM combined with a 20% overhead HD-FEC can be employed for a net data rate of 5 Gbps. Alternatively, a lower complexity HD-FEC with an overhead of 6.7% can be paired with 32-QAM for a net data rate of 4.7 Gbps. The multi-modulation format software-defined DSP allows for efficient operation from 5 dB up to 25 dB OSNR, flexibly switching modulation format depending on OSNR.

## V. DISCUSSION

Fig. 8 shows the GS formats used in this work. Both GS-8-QAM and GS-128-QAM are optimized for the AWGN channel at SNR values of 14 dB and 20 dB, respectively. The optimization uses an iterative approach similar to [18]. The constellations are initialized using the conventional layout and optimized by iterating between adding perturbations in the form of Gaussian noise to a randomly chosen single point and swapping the binary labels of two randomly chosen constellation points until convergence is reached. After each iteration, the generalized mutual information (GMI) is evaluated and if

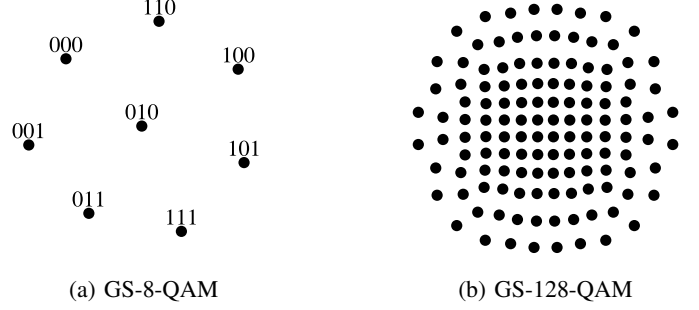


Fig. 8: Employed geometrically-shaped constellations.

gains are found, the modified constellation is taken as the new baseline.

GS formats for various SNR values were created and tested. Only the GS-8-QAM at 14 dB SNR and GS-128-QAM at 20 dB show significant gain over their conventional counterparts and are included in this work. Note that this technique optimizes for a different channel than the one employed in this work. Therefore, it is expected that more advanced optimization techniques taking into account the channel including CSNR and KK reconstruction errors will produce better performing constellations. Here, we included these suboptimal constellations as a proof-of-concept for using GS formats in the flexible multi-modulation format receiver and to show that gain in terms of OSNR tolerance can be achieved using GS.

In [11] we noted that the error floor or Q-factor ceiling of high-cardinality formats is most likely due to low-pass filtering at the receiver causing KK reconstruction errors. Here, we use a photodiode with higher bandwidth, enabling successful processing of 64-QAM signals reaching the 20% HD-FEC Q-factor threshold. Further gains could be made by employing a higher bandwidth ADC as well. Note that the KK reconstruction errors are caused by filtering effects between direct detection at the photodiode and conversion in the ADC [20]. Alternatively, one could implement a second static equalizer before the KK algorithm to counter these filtering effects [21].

The main factor limiting baud and data rates in this work is the ADC. The off-the-shelf commercial 12-bit 4 GS/s ADC uses an eight-lane PCIe Gen 3 interface to communicate with the GPU. This interface limits the sampling rate of the ADC. Future ADCs, employing PCIe Gen 4 or additional lanes, are expected to offer greater sampling rates and bandwidth. Proprietary interfaces such as NVIDIA NVLink, at the time of writing not available on off-the-shelf ADCs, can support an order of magnitude higher throughput from ADC to GPU and may enable greater increases in sampling rates.

## VI. CONCLUSION

A commercial off-the-shelf GPU is used for real-time digital signal processing of minimum-phase 4-, 8-, 16-, 32-, 64-, and 128-QAM as well as geometrically-shaped 8-QAM and 128-QAM signals detected with a KK coherent receiver [15]. This real-time, flexible, multi-modulation format receiver is experimentally validated using a field-deployed link between



two Tokyo locations. A net data rate of 5 Gbps is demonstrated using 1 GBaud 64-QAM. This shows the potential of GPUs for software-defined signal processing functionality in optical communication systems.

## REFERENCES

- [1] S. Beppu, K. Igarashi, H. Mukai, *et al.*, "Real-time strongly-coupled 4-core fiber transmission," in *Optical Fiber Communication Conference (OFC) 2020*, Optical Society of America, 2020, Th3H.2. DOI: 10.1364/OFC.2020.Th3H.2.
- [2] S. Beppu, K. Igarashi, M. Kikuta, *et al.*, "Weakly coupled 10-mode-division multiplexed transmission over 48-km few-mode fibers with real-time coherent MIMO receivers," *Opt. Express*, vol. 28, no. 13, pp. 19 655–19 668, Jun. 2020. DOI: 10.1364/OE.395415.
- [3] S. Randel, S. Corteselli, D. Badini, *et al.*, "First real-time coherent MIMO-DSP for six coupled mode transmission," in *2015 IEEE Photonics Conference (IPC)*, 2015. DOI: 10.1109/IPCon.2015.7323761.
- [4] R. Li, J. Zhou, Y. Dou, *et al.*, "A multi-standard efficient column-layered LDPC decoder for Software Defined Radio on GPUs," in *2013 IEEE 14th Workshop on Signal Processing Advances in Wireless Communications (SPAWC)*, 2013, pp. 724–728. DOI: 10.1109/SPAWC.2013.6612145.
- [5] T. Suzuki, S. Kim, J. Kani, *et al.*, "Demonstration of 10-Gbps Real-Time Reed–Solomon Decoding Using GPU Direct Transfer and Kernel Scheduling for Flexible Access Systems," *Journal of Lightwave Technology*, vol. 36, no. 10, pp. 1875–1881, 2018. DOI: 10.1109/JLT.2018.2793938.
- [6] T. Suzuki, S. Kim, J. Kani, *et al.*, "10-Gb/s Software Implementation of Burst-Frame Synchronization Using Array-Access Bitshift and Dual-Stage Detection for Flexible Access Systems," *Journal of Lightwave Technology*, vol. 36, no. 23, pp. 5656–5662, 2018. DOI: 10.1109/JLT.2018.2870912.
- [7] T. Suzuki *et al.*, "Software Implementation of 10G-EPON Upstream Physical-Layer Processing for Flexible Access Systems," *J. of Lightw. Technol.*, vol. 37, no. 6, pp. 1631–1637, Mar. 2019.
- [8] T. Suzuki, S. Kim, J. Kani, *et al.*, "Demonstration of Fully Softwarized 10G-EPON PHY Processing on a General-Purpose Server for Flexible Access Systems," *Journal of Lightwave Technology*, vol. 38, no. 4, pp. 777–783, 2020. DOI: 10.1109/JLT.2019.2948333.
- [9] T. Suzuki *et al.*, "Real-Time Implementation of Coherent Receiver DSP Adopting Stream Split Assignment on GPU for Flexible Optical Access Systems," *J. of Lightw. Technol.*, vol. 38, no. 3, pp. 668–675, Feb. 2020.
- [10] S. van der Heide, R. S. Luis, B. J. Puttnam, *et al.*, "Real-time, Software-Defined, GPU-Based Receiver Field Trial," *ECOC We1E5*, 2020.
- [11] S. van der Heide, R. S. Luis, B. J. Puttnam, *et al.*, "Field Trial of a Flexible Real-Time Software-Defined GPU-Based Optical Receiver," *J. Lightwave Technol.*, vol. 39, no. 8, pp. 2358–2367, Apr. 2021.
- [12] S. van der Heide, R. S. Luis, B. J. Puttnam, *et al.*, "10,000 km Straight-line Transmission using a Real-time Software-defined GPU-Based Receiver," *arXiv:2104.06311 [CHECK WHETHER THE OFC PAPER IS OUT ON IEEE XPLORE]*, 2021.
- [13] P. J. Winzer and D. T. Neilson, "From Scaling Disparities to Integrated Parallelism: A Decathlon for a Decade," *J. of Lightw. Technol.*, vol. 35, no. 5, pp. 1099–1115, Mar. 2017.
- [14] Y. Sun *et al.*, "Summarizing CPU and GPU Design Trends with Product Data," *en, arXiv:1911.11313 [cs]*, Nov. 2019, arXiv: 1911.11313.
- [15] A. Mecozzi, C. Antonelli, and M. Shtaif, "Kramers Kronig coherent receiver," *en, Optica*, vol. 3, no. 11, p. 1220, Nov. 2016. DOI: 10.1364/OPTICA.3.001220.
- [16] E. P. da Silva and D. Zibar, "Widely Linear Equalization for IQ Imbalance and Skew Compensation in Optical Coherent Receivers," *Journal of Lightwave Technology*, vol. 34, no. 15, pp. 3577–3586, 2016.
- [17] R. S. Luis, G. Rademacher, B. J. Puttnam, *et al.*, "Simple method for optimizing the DC bias of Kramers-Kronig receivers based on AC-coupled photodetectors," *Opt. Express*, vol. 28, no. 3, pp. 4067–4075, Feb. 2020. DOI: 10.1364/OE.383369.
- [18] B. Chen, C. Okonkwo, D. Lavery, *et al.*, "Geometrically-shaped 64-point constellations via achievable information rates," in *2018 20th International Conference on Transparent Optical Networks (ICTON)*, 2018, pp. 1–4. DOI: 10.1109/ICTON.2018.8473932.
- [19] E. Agrell and M. Secondini, "Information-Theoretic Tools for Optical Communications Engineers," in *2018 IEEE Photonics Conference (IPC)*, IEEE, Sep. 2018, pp. 1–5. DOI: 10.1109/IPCon.2018.8527126.
- [20] X. Chen, C. Antonelli, S. Chandrasekhar, *et al.*, "Kramers–Kronig receivers for 100-km datacenter interconnects," *Journal of Lightwave Technology*, vol. 36, no. 1, pp. 79–89, 2018. DOI: 10.1109/JLT.2018.2793460.
- [21] X. Chen, S. Chandrasekhar, S. Olsson, *et al.*, "Impact of O/E Front-End Frequency Response on Kramers-Kronig Receivers and its Compensation," in *2018 European Conference on Optical Communication (ECOC)*, 2018, pp. 1–3. DOI: 10.1109/ECOC.2018.8535239.

**Sjoerd van der Heide** (S'13) was born in 's-Hertogenbosch, the Netherlands, in 1992. He received the B.Sc. and M.Sc. (cum laude) degrees in Electrical Engineering from Eindhoven University of Technology, the Netherlands, in 2015 and 2017, respectively. He is currently working towards a PhD degree at the High Capacity Optical Transmission Laboratory, Electro-Optical Communications group, at Eindhoven University of Technology. His research interests include space-division multiplexing and digital signal processing. He is the recipient of a student paper award at ECOC 2018, a best paper award at OECC 2019, and a student paper award at ECOC 2020.

**Ben Puttnam** (M'12) is a senior researcher in the Photonic Network System Laboratory at the National Institute of Information and Communications Technology (NICT) in Tokyo, Japan. He received the MPhys degree in Physics from the University of Manchester (UK) in 2000 and the PhD degree from University College London in 2008, working as a Switch Design Engineer for T-mobile (UK) in between. After short term visits to NICT, supported by JSPS and the Photonics group at Chalmers University, Göteborg, Sweden supported by the Ericsson research foundation he re-joined NICT in March 2010. His research interests are space-division multiplexing for optical transmission and optical signal processing.

**Georg Rademacher** (M'14, SM'20) received the Dipl.-Ing. and Dr.-Ing. degree in electrical engineering from Technische Universität Berlin, Germany, in 2011 and 2015, respectively. During his doctoral studies, he did internships at Bell Laboratories in Holmdel, USA and the National Institute of Information and Communications Technology (NICT) in Japan. In 2016 he joined the Photonic Network System Laboratory at NICT in Tokyo, Japan, where he is engaged in research on subsystems and systems for efficient high capacity optical transmission.

**Chigo Okonkwo** (M'09–SM'18) was born in Wakefield, U.K., in 1979. He received the Ph.D. degree in optical signal processing from the University of Essex, Colchester, U.K., in 2010. Between 2003 and 2009, he was a Senior Researcher with the Photonic Networks Research Lab, University of Essex, U.K. After his Ph.D., he was appointed as a Senior Researcher with the Electro-optical communications group working on digital signal processing techniques and the development of space division multiplexed transmission (SDM) systems. He is currently an Associate Professor and leads the High-capacity optical transmission laboratory within the Institute for Photonic Integration, Department of Electrical Engineering, Eindhoven University of Technology (TU/e), The Netherlands. He was instrumental to the delivery of the first major SDM project in the European Union—MODEGAP project. Since 2014, he has been tenured at the ECO group, where he has since built up a world-class laboratory collaborating with several industrial and academic partners. His general research interests are in the areas of optical and digital signal processing, space division multiplexing techniques, and long-haul transmission techniques. In 2018, he was TPC chair for subcommittee 3 on digital signal handling. Between 2015 and 2017, he served on the TPC for the OSA conference on signal processing in photonic communications (SPPCom). In 2017 and 2018, he was the Program Chair and the Conference Chair at SPPCom, respectively. Dr. Okonkwo recently served as an associate editor for special edition of the IEEE Journal on Lightwave Technology. For the next 3 years, he has been retained to serve as technical programme subcommittee on Fiber-optic and waveguide devices and sensors (subcommittee D5) at Optical fiber communications conference OFC 2020-2022.

**Satoshi Shinada** (Member, IEEE) received the B.S. degree from Science University of Tokyo in 1998 and the M.E. and Ph.D. degrees from Tokyo Institute of Technology in 2000 and 2002, respectively. In 2002 he joined the Precision and Intelligence Laboratory, Tokyo Institute of Technology as a JSPS Post-Doctoral Fellow. Since 2003, he has been with National Institute of Information and Communications Technology (NICT), Tokyo Japan. From 2015 to 2016, he was a Deputy Director of the Ministry of Internal Affairs and Communications, Japan. He has been engaged in the research and development on LiNbO<sub>3</sub> optical modulators, optical switches, optical interfaces for single flux quantum circuit and optical packet switching (OPS) systems. Dr. Shinada received the IEEE/LEOS Student Award in 2002, and the 2015 Ichimura Prize in Science for Excellent Achievement from the New Technology Development Foundation. He is a member of IEEE, IEEE Photonics Society, the Japan Society of Applied Physics (JSAP) and the Institute of Electronics, Information and Communication Engineers of Japan (IEICE).